Heliyon 9 (2023) e21578

Contents lists available at ScienceDirect

Heliyon

journal homepage: www.cell.com/heliyon

Evaluation of CMIP6 model performance and extreme precipitation prediction in the Awash basin

Chala Hailu Sime *, Wakjira Takala Dibaba

Department of Hydraulic and Water Resources Engineering, Jimma University, Jimma, 378, Ethiopia

ARTICLE INFO

Keywords:
Awash basin
Best fit
CMIP6
Extreme precipitation
General extreme value

ABSTRACT

Extreme rainfall and its accompanying hydrological extremes are happening more frequently as a result of global warming's alteration of regional and local weather patterns. This poses a serious risk to ecosystem, environment and the community livelihoods. The Awash basin in Ethiopia is especially vulnerable to these events, posing significant threats to the region. There are, however, limited information's available that could be used to characterize the condition of extreme precipitation in the basin. Therefore, this study aims to evaluate the performance of CMIP6 models in simulating extreme precipitation in the Awash basin. Additionally, the study calculated extreme precipitation using best-fit probability distribution functions (PDFs) for the period from 1985 to 2014. The Climate Hazards Group Infrared Precipitation with station data (CHIRPS) were used to evaluate the global climate models. Simulated data were interpolated using bilinear techniques. Four statistical indices (percentage of bias, root mean square error, mean absolute error, and Pearson correlation) assessed GCM performance in simulating precipitation extremes. Graphical approaches, numerical methods, and empirical distribution functions were employed to evaluate the performance of various probability distribution functions (PDFs). The study identified MIROC6, CESM2-WACCM, and Ensemble as well-performing models with PBIAS and RMSE of 6.6 %, −10.2 %, −17.2 %, and 11.5, 10, 9.7 respectively, while MPI-ESM1-2-HR and EC-Earth3 struggled with extreme rainfall simulation. The generalized extreme values distribution was found to be a good fit for extreme rainfall estimation. GFDL-ESM4 and BCC-CSM2-MR models estimated the highest extreme rainfall of 90 mm/day and 80 mm/day, respectively, however these models overestimated the return period. Conversely, MRI-ESM2-0, NorESM2-MM, ACCESS ESM1-5, and CMCC-ESM2 models underestimated the return periods. Spatially, GFDL-ESM4 and ACCESS-ESM1-5 models exhibited uniform peak rainfall values over a large area. Overall, the study suggests that employing the generalized extreme value distribution could effectively inform risk assessment and management of extreme events in the Awash basin.

1. Introduction

Burning of fossil fuels in various sectors causes GHG emissions, and it is one of the reason of global warming [1–3]. The global warming has led to notable shifts in global climate patterns, resulting in increased occurrences of extreme climatic events [4–6]. Climate change-induced droughts and floods caused by intense rainfall events have been on the rise worldwide, posing significant

* Corresponding author.
E-mail address: chalahailuu@gmail.com (C.H. Sime).

https://doi.org/10.1016/j.heliyon.2023.e21578
Received 15 July 2023; Received in revised form 20 October 2023; Accepted 24 October 2023
Available online 31 October 2023

List of abbreviations

CDO	Climate Data Operator
CHIRPS	Climate Hazards Group Infrared Precipitation With Station Data
CMIP	Coupled Model Intercomparison Project
GEV	Generalized Extreme Value
MAE	Mean Absolute Error
MLE	Maximum Likelihood Estimation
PBIAS	Mean Percentage Of Bias
PDFs	Probability Distribution Functions
r	Pearson Correlation
RMSE	Root Mean Square Error
SPPs	Shared Socioeconomic Pathways

challenges in various countries [7,8]. Such extreme rainfall has been observed to trigger flooding and landslides, leading to substantial disruptions to social, economic, and political activities within affected communities [9]. Developing countries, including those in Africa like Ethiopia, face particular vulnerability due to their limited adaptability and resilience to natural disasters. The Awash River Basin in Ethiopia, in particular, has experienced recurring and devastating droughts and floods, resulting in famine, population displacement, and the destruction of infrastructure and the environment [10,11]. However, limited research has been conducted on evaluating how general circulation models (GCMs) accurately reproduce the historical climate patterns of Ethiopia, especially the Awash basin, to devise a proper strategy for climate change adaptation and mitigations.

Extreme rainfall events represent the highest levels of precipitation expected within a specific time frame. The latest climate projections indicate an increase in the occurrence of such extreme rainfall events, particularly in regions with complex topography that can amplify rainfall variability [12,13]. These extreme climatic events play a crucial role in determining the frequency of their occurrence, which is often expressed as a recurrence interval. To analyze extreme rainfall patterns, researchers commonly employ various probability distribution functions (PDFs) such as Normal, Log-normal, Exponential, Gamma, Gumbel, Weibull, and Generalized Extreme Value (GEV) [14–16]. These PDFs are used in hydrological research to explore extreme occurrences utilizing different recurrence intervals, such as 5, 10, 25, 50, and 100 years [12,16].

Historical climate model simulations are primarily serve to assess the models' abilities in simulating average and extreme precipitation [17] as well as precipitation and temperature patterns [18]. To enable standardized climate simulations, model comparisons, and review process, the World Climate Research Programme (WCRP) established the Coupled Model Intercomparison Project (CMIP). Over time, CMIP has undergone five phases and has become a crucial component of national and global climate change assessments [19]. A new simulation framework is presented in the most recent phase, CMIP6. To choose the most appropriate climate models, however, a comprehensive evaluation of multi-model performance is required when it comes to climate projections and extreme events.

With the expansion in both the quantity and range of experiments, CMIP6 has adopted a more decentralized structure to facilitate evaluation and intercomparison of models for standardized climate simulations. Compared to earlier iterations such as CMIP5 and CMIP3, CMIP6 Global Climate Models exhibit notable advancements in spatial resolution, physical parameterizations (including improved representation of clouds), and the incorporation of additional Earth system processes (like nutrient constraints on the terrestrial carbon cycle) and components (such as ice sheets) [19]. CMIP6 surpasses CMIP5 in terms of the number of participating modeling groups, the range of future scenarios examined, and the diversity of experiments conducted [20]. Despite differences between models and observations, CMIP6 exhibits considerably superior ability in simulating precipitation, potential changes in precipitation [21,22]. However, a comprehensive investigation is still necessary to ascertain the improvements made by CMIP6 models in simulating precipitation and its extremes across various spatial and temporal scales.

Despite the advancements and effectiveness of the current CMIP6 models combined with Shared Socioeconomic Pathways (SSPs), there remains limited information available on projected precipitation extremes specifically for Ethiopia and the Awash River basin. Additionally, there is a scarcity of studies focusing on multimodal General Circulation Models (GCMs) from earlier CMIP generations for climate change research in Ethiopia and the Awash basin. While there have been some studies on the entire Awash basin, such as examining the impacts of climate change on the hydrology of the Awash river basin [23] and the effects of climate change on water resources in the Awash [24], there exist discrepancies in precipitation predictions between these studies. The projected precipitation trends over the Awash basin exhibit significant variability, with some studies indicating an average annual increase of over 10 % using Global and Regional Climate Models [23].

To compare and evaluate probability distribution function (PDF) sets in extreme rainfall assessments, it is essential to consider long-term data and compare them with other climatic datasets available in CMIP6. The suitability of a PDF in representing extreme rainfall can be determined through goodness-of-fit tests, which evaluate the consistency between observed maximum annual daily rainfall and the PDF. Several tests, including the Kolmogorov-Smirnov (K–S) test, Anderson-Darling (A-D) test, and chi-square test (S-Q), have been utilized in previous studies to identify the best-fitting PDFs [9,12,25,26]. In these studies, individual PDFs were assessed using these tests, and the total test score was calculated by combining the outcomes of all three techniques to determine the best-fit PDF. Additional methods such as quantile-quantile (Q-Q) plots, skewness, and kurtosis indices can also be employed to evaluate the

performance of the PDFs. Skewness provides information about the direction and magnitude of the PDF are measured by skewness. The Kurtosis represents the idea of flatness, while the skewness represents how far the frequency distribution deviates from symmetry and in which direction (positive or negative). Kurtosis helps to provide a complete image of the distribution's form.

The parameters of the probability distribution function (PDF) can be estimated through various methods such as the L-moment method, maximum likelihood estimation (MLE) method, and nonlinear least squares methods [9,12,27]. Among these methods, the maximum likelihood estimation method is commonly preferred [18,26,28]. In the maximum likelihood approach, a probability function is constructed, and the model parameters are adjusted to maximize the likelihood of obtaining the observed dataset.

Researchers and policymakers are eager to understand the accuracy of the latest CMIP6-GCMs in representing global and regional climate patterns, as well as the potential changes in extreme precipitation under new emissions scenarios. To address the issues posed by climate change, this framework encourages the creation of policies and informed decision-making. In order to develop effective mitigation and adaptation measures, it is important to link emissions to specific climate consequences through the assessment of extreme precipitation [19,29–31]. Hence, this study aimed to evaluate the performance of GCMs in CMIP6 regarding the simulation of extreme precipitation. Reliable assessments of extreme rainfall are valuable for multiple purposes, including the design of hydraulic and flood protection structures. They enable the determination of rainfall frequency, comparison of different approaches to predicting design rainfall, and estimation of the risks associated with extreme damage. Therefore, the research findings from this study provide valuable insights to inform water resource policymakers and decision-makers, enabling them to make informed and improved decisions.

Given the above-stated needs and significance, the goal of this study was to evaluate the performance of CMIP6 models in simulating extreme precipitation in the Awash basin. The procedures used include interpolating CMIP6 grid data to stations using bilinear interpolation techniques. The model's performance in rainfall simulation utilizing CHIRPS data was then evaluated using statistical methods. To assess the effectiveness of various probability distribution functions (PDFs), graphical approaches, numerical methods, and empirical distribution functions were used. Finally, how well the CMIP6 models performed in simulating extreme precipitation were presented using the PDFs. Conducting simulations of extreme precipitation events using CMIP6 models represents a pivotal step in advancing our ability to foresee and respond to future climate challenges. These endeavors not only enhance our comprehension of the intricate processes governing extreme precipitation, but also provide invaluable information for policymakers, resource managers, and communities to develop robust strategies for climate resilience and mitigation. The integration of cutting-edge modeling techniques with satellite data further solidifies the scientific foundation for informed decision-making in the face of an evolving climate system.

2. Material and method

2.1. Location of the study area

The Awash River Basin is a substantial river basin located in Ethiopia and renowned for its size. It spans across the geographical coordinates of 37.96°–43.27° E and 7.9°–12.39° N. The source of the Awash River is the near town of Ginichi town, west of Addis Ababa, Ethiopia. It meanders through the country until it reaches Lake Abe Afar. The river basin encompasses a vast area of approximately 112,000 square kilometers. As a perennial river, it maintains a consistently high streamflow. The Awash River Basin is home to numerous significant projects, including major hydropower facilities and irrigation schemes for sugar production. With an elevation ranging from 74 to 4193 m above sea level, the study area exhibits a diverse topography. The basin is characterized by four distinct climate zones: Hot, Warm, Tepid, Cool, and Very cool. The central and downstream regions primarily experience a hot climate, while the largest portion of the basin falls within the hot zone. In contrast, the very cool climate covers a smaller area [32]. The average annual rainfall in the region varies, with downstream areas receiving around 200 mm, while higher elevations in the highlands

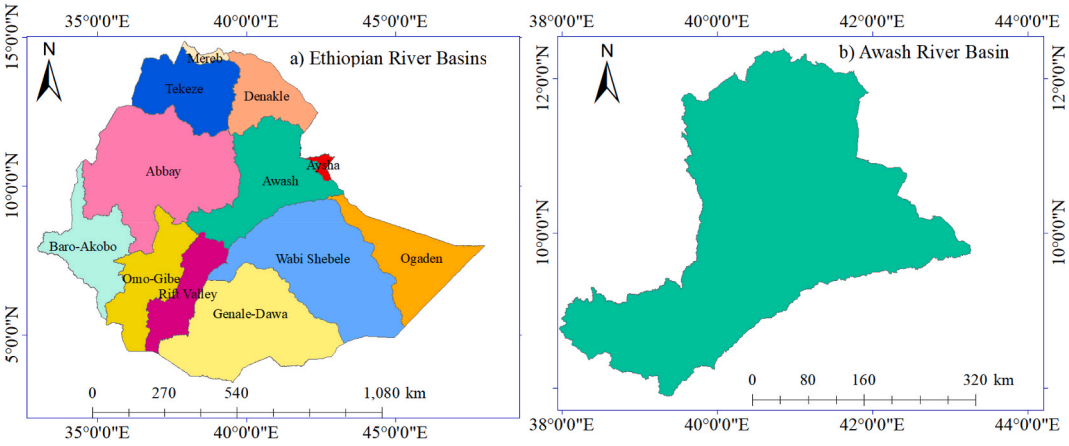

Fig. 1. Location map of Ethiopian River Basins (a) and Awash River basin (b).

experience approximately 1600 mm of rainfall [23]. Fig. 1a portrays the Ethiopian River Basins, with Fig. 1b specifically highlighting the Awash River Basin as a distinct area of interest. The figures serve to provide a visual representation of the study area and its geographical context.

2.2. Data

The daily precipitation data of 12 CMIP6 models were acquired from the official website of the Earth System Grid Federation's data portals (ESGF) CMIP6 archives, which can be accessed at https://esgf-node.llnl.gov/projects/cmip6/. The historical simulations of precipitation data spanning from 1850 to 2014 were utilized to assess the performance of the GCMs.

As a reference for evaluating the historical simulations of CMIP6 GCMs, observed precipitation data sets from the Climate Hazards Group Infrared Precipitation with Station data (CHIRPS) were employed. CHIRPS was selected among the existing datasets due to its recognized accuracy over Ethiopia, as confirmed by previous studies conducted by Almazroui et al. [33] and Dinku et al. [34]. The detail characteristics of the 12 GCMs used in this study is presented in Table 1. A set of criteria was created to identify GCMs that could be appropriate for the study area before choosing the candidate GCMs. As the study is on a basin scale, a nominal resolution of 100 km was set first. In addition, as the study involves performance evaluation, only GCMs with first member realization (r1i1plf1) were used i.e. only models having similar variant label is used in order to have an unbiased comparison of all of them. In this case, models with different variant label are not considered for comparisons, as models with different variant label can be associated to different realization, initialization and characteristics. Accordingly, 12 GCMs were selected for this study. Moreover, these models were also evaluated in different parts of the world to see how well they simulated rainfall. They performed better compared to other models, as mentioned in the studies by Refs. [35–37].

2.3. Interpolating CMIP6 grid data to stations

To obtain station data from the grid data, interpolation techniques are employed. The widely utilized method for this purpose is bilinear interpolation, as described by Zhou and Zhao [38]. Bilinear interpolation involves utilizing information from neighboring cells surrounding a particular point, both in weighted and non-weighted systems. In this process, four nearest neighbors are considered, as outlined by Ramesh et al. [39]. The Climate Data Operator (CDO) program was utilized to perform these interpolation tasks. The CDO software consists of a set of operators designed to effectively handle climate and forecast model data in a consistent manner.

2.4. Methods/model performance criteria

Before conducting the performance analysis, all CMIP6 outputs and observational data were adjusted to a standardized spatial resolution of $1^\circ \times 1^\circ$ using bilinear interpolation techniques. This re-gridded data, with a consistent spatial resolution, was utilized to evaluate the model performance. In assessing the capability of CMIP6 models to simulate extreme precipitation compared to CHIRPS data, Mean Percentage of Bias (PBIAS), Root Mean Square Error (RMSE), Mean Absolute Error (MAE), and Pearson Correlation (r) were employed [40,41]. A smaller absolute value of RMSE and BIAS indicates better model performance, while a larger value of r, ranging from −1 to 1, suggests improved correlation between the simulated and observed climate variables. A value close to 0 indicates poor model performance with weak correlation [42–44] D. The specific equations utilized for calculating BIAS, RMSE, r, and MAE are presented in equations (1)–(4), respectively.

$$\mathrm{BIAS} = \frac{\sum_{i=1}^{n} (\mathrm{Si} - \mathrm{Oi})}{\sum_{i=1}^{n} (\mathrm{Oi})} * 100 \tag{1}$$

Table 1
The modeling center and country, model name, and atmospheric resolution of the 12 CMIP6 global climate models were used in this study.

Modeling center and country	Model name	Resolution
Australian Community Climate and Earth System Simulator-ACCESS	ACCESS-ESM1-5	$1.9^\circ \times 1.2^\circ$
Beijing Climate Center and China meteorological Administration, China	BCC-CSM2-MR	$1.13^\circ \times 1.13^\circ$
National Centre for Atmospheric Research, USA	CESM2-WACCM	$1.25^\circ \times 0.94^\circ$
Euro-Mediterranean Centre on Climate Change- Earth System Model	CMCC-ESM2	$1.25^\circ \times 0.94^\circ$
EC-Earth Consortium, Sweden	EC-Earth3	$0.70^\circ \times 0.70^\circ$
National Oceanic and Atmospheric Administration, Geophysical Fluid Dynamics Laboratory (GFDL), USA	GFDL-CM4	$1.25^\circ \times 1^\circ$
National Oceanic and Atmospheric Administration, Geophysical Fluid Dynamics Laboratory (GFDL), USA	GFDL-ESM4	$1.25^\circ \times 1^\circ$
Institute for Numerical Mathematics, Russian Academy of Science, Russia	INM-CM5-0	$2^\circ \times 1.5^\circ$
Japan Agency for Marine-Earth Science and Technology, Japan	MIROC6	$1.41^\circ \times 1.41^\circ$
Max Planck Institute for Meteorology, Germany	MPI-ESM1-2-HR	$0.94^\circ \times 0.94^\circ$
Meteorological Research Institute (MRI), Japan	MRI-ESM2-0	$1.13^\circ \times 1.13^\circ$
Norwegian Climate Centre, Norway	NorESM2-MM	$1.25^\circ \times 0.94^\circ$

$$RMSE = \sqrt{\frac{1}{n}\sum_{i=1}^{n}(Si - Oi)^2} \tag{2}$$

$$r = \frac{\sum_{i=1}^{n}(Si - Sm)(Oi - Om)}{\sqrt{\sum_{i=1}^{n}(Si - Sm)^2}\sqrt{\sum_{i=1}^{n}(Oi - Om)^2}} \tag{3}$$

$$\mathrm{MAE} = \sum_{i=1}^{n}\frac{|P_i - O_i|}{N} \quad 4$$

where S_i is simulated, and O_i is the observed value of the climate variable, *i* refers to the simulated and observed pairs, n is the total number of the pairs, and m refers to mean extreme rainfall.

2.5. Probability density functions (PDF)

In order to assess the extreme precipitation simulated by CMIP6 across the Awash River basin, a commonly used probability density function (PDF) in extreme precipitation studies was selected. Specifically, the Generalized Extreme Value (GEV), Normal, log-normal, Gumbel, and Weibull distribution methods were chosen. These distribution methods were selected due to their widespread utilization in the assessment of extreme precipitation in various regions worldwide.

2.5.1. Generalized extreme value (GEV)

The analysis of extreme rainfall and its corresponding probability density functions (PDFs) was conducted using the Generalized Extreme Value (GEV) distribution method, using the yearly maximum daily rainfall data from the best-performing CMIP6 model. In the GEV approach, extreme rainfall (X_T) is assessed for a selected return period (T). The GEV distribution method relies on parameters such as the position parameter (γ), scale parameter (α), and shape parameter (k) [45,46]. The cumulative distribution function (CDF), denoted as F(x), and the probability density function (PDF), denoted as f(x), for the Generalized Extreme Value (GEV) can be expressed using equations (5) and (6).

$$f(x) = \frac{1}{\beta}\left[\left(1 - \alpha\left(\frac{x - \gamma}{\beta}\right)\right)^{\frac{1}{\alpha - 1}}\exp\left\{-\left(1 - \alpha\left(\frac{x - \gamma}{\beta}\right)\right)^{1/\alpha}\right\}\right] \tag{5}$$

$$F(x) = \exp\left\{-\left(1 - \alpha\left(\frac{x - \gamma}{\beta}\right)\right)^{1/\alpha}\right\} \tag{6}$$

2.5.2. Normal distribution (ND)

The ND is used in annual maximum precipitation and runoff analysis. (Mean (μ) and standard deviation (σ) are the parameters of the ND. The PDF, f(x) and CDF, F(x) for a normal random variable x are expressed [47] as in equations (7) and (8).

$$f(x) = \frac{1}{\delta\sqrt{2\pi}}exp\left[-\frac{1}{2\delta^2}(x - \mu)^2\right] \quad for - \infty < x < \infty \tag{7}$$

$$F(x) = \frac{1}{\delta\sqrt{2\pi}}\int_{-\infty}^{\infty}\exp\left[-\frac{1}{2\delta^2}(x - \mu)^2\right]dx \tag{8}$$

2.5.3. Log-normal distribution

It is a random variable distribution at which the normal distribution is the logarithm. The PDF and CDF of the log-normal distribution are given in Equations (9) and (10) [12].

$$f(x) = \frac{1}{x\sigma_{\log(x)}\sqrt{2\pi}}\ exp\left\{-\frac{1}{2}\left[\frac{\log(x) - \mu_{\log(x)}}{\sigma_{\log(x)}}\right]^2\right\} for\ x > 0 \tag{9}$$

$$F(x) = \int_{-\infty}^{x}\frac{1}{x\sigma_{\log(x)}\sqrt{2\pi}}\ exp\left\{-\frac{1}{2}\left[\frac{\log(x) - \mu_{\log(x)}}{\sigma_{\log(x)}}\right]^2\right\} for\ x > 0 \tag{10}$$

where x is the variable under consideration, $f(x)$ is the probability of the variable being lower or equal to the random variable x, μ is the average of x, and σ is the standard deviation of x.

2.5.4. Gamma distribution

For shape parameter $(\alpha > 0)$ and $(\beta > 0)$ scale parameters of the random variable x, the gamma probable density function can be

expressed as in Equations (11) and (12) [48].

$$f(x) = \frac{1}{\beta^{\alpha}\Gamma(\alpha)} x^{\alpha-1} e^{\frac{-x}{\beta}} \quad for\ 0 < x < \infty \tag{11}$$

Were $\Gamma(\alpha)$ *is* gamma function
The CDF can be expressed as follows

$$F(x) = \frac{1}{\beta^{\alpha}\Gamma(\alpha)} \int_0^x \mu^{\alpha-1} e^{\frac{-x}{\beta}} dx \quad for\ 0 < x < \infty \tag{12}$$

The gamma parameters can be calculated using the maximum likelihood estimation method as shown in the equation as in equations (13) and (14) [49].

$$\alpha = \frac{1 + \sqrt{\frac{1+4\left(\log\left(\overline{x}\right) - x_g\right)}{3}}}{4\left(\log(\overline{x}) - x_g\right)} \tag{13}$$

$$\beta = \frac{\overline{x}}{\alpha} \tag{14}$$

Where $\overline{x}$ is the arithmetic mean and x_g is the geometric average of random variables?

2.5.5. Gumbel distribution

The PDF and PDF of Gumbel's probable density function can be expressed as in Equations (15) and (16) [49,50].

$$f(x) = \frac{1}{\beta} e^{\left(\frac{x-\gamma}{\beta}\right)} - e^{-e^{\left(\frac{x-\gamma}{\beta}\right)}} \tag{15}$$

$$F(x) = e^{\pm e^{\left(\frac{x-\gamma}{\beta}\right)}} \tag{16}$$

2.5.6. Weibull distribution

The Weibull distribution function can be given for PDF and CDF as in equations (17) and (18) [49,51,52].;

$$f(x) = \frac{\alpha}{\beta}\left(\frac{x-\gamma}{\beta}\right)^{\alpha-1} e^{-\left(\frac{x-\gamma}{\beta}\right)^{\alpha}} \tag{17}$$

γ is the location parameter, α is the shape parameter, and β is the scale parameter.
The Weibull CDF can be estimated using the equation,

$$\mathrm{F(x)} = \frac{1}{\beta}\int_0^{\infty} f(x)dx = e^{-\left(\frac{x-\alpha}{\beta}\right)^{\gamma}} \tag{18}$$

2.6. Skewness and Kurtosis

Kurtosis and skewness are used to analyze the performance of PDF. Skewness and Kurtosis can be determined by equations (19) and (20) [9].

$$k = \frac{n^2}{(n-1).(n-2).(n-3)} . \frac{\sum_{i=1}^{n}(x_i - \overline{x})^4}{s^4} \tag{19}$$

$$g = \frac{n}{(n-1).(n-2)} . \frac{\sum_{i=1}^{n}(x_i - \overline{x})^3}{s^3} \tag{20}$$

where n is series length, s is standard deviation, x_i is individual random variables, $\overline{x}$ is an average of individual variables, k is Kurtosis, g is skewness.

2.7. The goodness of fit (GOF) tests

The adequacy of a probability distribution model is evaluated using statistical measures, referred to as the goodness-of-fit (GOF)

tests. Three different approaches, namely graphical methods, numerical methods, and the empirical distribution function (EDF), are employed to assess the performance of the selected probability distribution function. EDF tests specifically measure the inconsistency between the observed (empirical) distribution and the theoretical distribution. Widely recognized EDF tests include the Kolmogorov-Smirnov (KS) test, the Anderson-Darling (AD) test, and the Chi-Square (CS) test [12].

2.7.1. Chi-square test (CS) test

Used to compare an observed distribution with the theoretical distribution intended by the PDF between the sum of squares [16, 26]. The C–S test method can be given by equations (21) and (22)

$$CS = \sum_{i=1}^{k} \left[\frac{(o_i - E_i)^2}{E_i} \right] \tag{21}$$

$$E_i = F(x_{i+1}) - F(x_i) \tag{22}$$

where oi is the number of observed annual maximum daily rainfall in class I, Ei is the expected number of annual maximum daily rainfall calculated by various distributions, i is the number of classes (1, 2, …, k), F is the cumulative density function (CDF) of the probability distribution being tested.

2.7.2. Kolmogorov-Smirnov (KS) test

The Kolmogorov-Smirnov (K–S) test was employed to quantify the disparity between the observed distribution and the assumed distribution. The empirical distribution function (EDF) was compared to the cumulative distribution function (CDF) to perform this test. The discrepancy between the EDF and CDF is represented by the KS test values. The overall process can be summarized as outlined in Refs. [53,54] and can be further understood by referring to equations (23)–(25)

$$f_x(x) = \begin{cases} 0; if\ X < X1 \\ \frac{k}{n}; if\ X_k \le X < X_{k+1} \\ 1; if\ X > X_n \end{cases} \tag{23}$$

Calculating the K–S statistics D_n.

$$D_n = max|F_x(x) - f_x(x)| \tag{24}$$

$$P(D_n \le D_n{}^{\alpha}) = 1 - \alpha \tag{25}$$

where $D_n{}^{\alpha}$ is a critical value α is a significant level, k is rank order data set.

2.7.3. Anderson-Darling (AD) test

In hydrologic extreme frequency analysis, the AD test emphasizes disparities in both distribution tails, typical of primary importance. The AD test is more appropriate in extreme rainfall analysis to check the best-fitted model to the maximum data. AD test can be calculated using equation (26) [54,55].

$$AD = -n - \frac{1}{n} \sum_{i=1}^{n} (2i - 1)\ [\ln(F(X_i) + \ln\ (1 - F((X_{n-i+1}))] \tag{26}$$

in this study, the selection of the most appropriate probability density functions (PDFs) was based on their ranking using the three aforementioned methods. The assessment of the likelihood of precipitation events occurring within specific time frames, such as the next 5 years, 10 years, 25 years, 50 years, and 100 years, was evaluated using the best-fit PDFs.

2.8. Spatial analysis of the climatological data

Precipitation data is fundamental in meteorological and hydrological studies; however, it may be limited or inaccessible due to a lack of meteorological stations or timely data availability. In such cases, interpolation techniques are commonly employed to estimate and map the spatial distribution of rainfall. Among various interpolation methods, Inverse Distance Weighting (IDW) is frequently utilized to generate distribution maps of meteorological parameters [56]. The IDW interpolation technique provides an estimation of precipitation distribution utilizing a mathematical equation, as described in Equation 27, 28 and 29 [57].

$$P_P = \sum_{i=1}^{N} W_i P_i \tag{27}$$

$$W_i = \frac{w_i}{\sum_{i=1}^{N} d_{pi}^{-m}} = \frac{d_{pi}^{-m}}{\sum_{i=1}^{N} d_{pi}^{-m}} \tag{28}$$

$$P_P = \frac{\sum_{i=1}^{N} P_i d_{pi}^{-m}}{\sum_{i=1}^{N} d_{pi}^{-m}} \tag{29}$$

where, P_P is the required rainfall data in mm, P_i is known rainfall data of the gauged station in mm, W_i is the weighting of individual rainfall stations w_i is a weighting factor that represents the relative importance of the individual rainfall station, i and N is the number of gauging stations, d_{pi} is the distance from each gauging station to the unknown site, m is the exponent, and the controlling factor.

3. Results and discussion

3.1. Performance of CMIP6 GCMs for extreme precipitation

In the extreme precipitation simulation, 12 CMIP6 were chosen to analyze the performance of GCMs over the Awash River basin. The models' average maximum daily precipitation was used for the performance analysis using CHIRPS observational data over the study area. The performance of the CMIP6 models' daily annual maximum precipitation concerning CHIRPS shows that most of the models underestimated the extreme precipitation in the Awash River Basin.

A negative PBIAS value indicates that the model underestimates extreme precipitation, and a positive PBIAS value indicates overestimation. As a result, BCC-CSM2-MR, GFDL-ESM4, GFDL-CM4, and MIROC6 overestimated extreme precipitation, whereas all other models examined underestimated the extreme precipitation. MPI-ESM1-2-HR and EC Earth3 failed to simulate extreme precipitation simulations; hence their simulation data were not included in the analysis and ensemble. The inverse relationship between the model simulation and CHIRPS data is shown by a negative correlation value (r), and a positive value of r represents the direct relation. Extreme precipitation simulated from models CESM2-WACCM, INM-CM5-0 and ACCESS-ESM1-5 positively correlate with CHIRPS data. The ensemble of 10 GCMs outperformance well in terms of RMSE, followed by MIROC6 and CESM2-WACCM, whereas the MIROC6 approach outperforms all statistical performance methods (Table 2). In line with this study, a better representation of the multi-model ensemble for extreme precipitation than the individual GCMs in CMIP6 was reported by Akinsanola et al. [17] over East Africa.

3.2. Kurtosis and skewness of extreme precipitation

Extreme precipitation with Platykurtic Kurtosis is found in BCC-CSM2-MR, CESM2-WACCM, GFDL-CM4, INM-CM5-0, ACCESS-ESM1-5, and Ensemble. Leptokurtic Kurtosis is found in CHIRPS, GFDL-ESM4, MRI-ESM2-0, NorESM2-MM, CMCC-ESM2, and MIROC6 (Table 3). Mesokurtic Kurtosis does not exist in any model. The data from GFDL-ESM4 and CMCC-ESM2 exhibit Kurtosis >3, indicating that they simulated intense precipitation with many heavy-tailed or outliers (Table 3).

Extreme precipitation in CHIRPS shows a negative skewness value near zero, indicating a slightly left tail in the distribution (slightly lower-class magnitude of precipitation); however, the other CMIP6 models had a right tail distribution (higher class magnitude of extreme precipitation). The skewness scores for CHIRPS, GFDL-CM4, MRI-ESM2-0, and ACCESS-ESM1-5, are between −0.5- and 0.5, indicating that extreme precipitation was reasonably symmetrical. The skewness values for models such as CESM2-WACCM, INM-CM5-0, NorESM2-MM, MIROC6, and Ensemble are moderately skewed between 0.5 and 1. BCC-CSM2-MR, GFDL-

Table 2
Performance of the CMIP6 in extreme rainfall simulations.

CMIP6 Models	Performance statistic			
	PBIAS	RMSE	r	MAE
BCC-CSM2-MR	19.3	17.0	−0.4	7.0
CESM2-WACCM	−10.2	10.0	0.1	3.7
GFDL-ESM4	21.5	16.4	−0.1	7.8
GFDL-CM4	29.4	16.5	−0.1	10.7
INM-CM5-0	−23.4	14.0	0.2	8.5
MRI-ESM2-0	−28.2	12.2	−0.1	10.2
NorESM2-MM	−30.9	13.8	−0.3	11.2
ACCESS-ESM1-5	−36.6	14.4	0.1	13.3
CMCC-ESM2	−37.2	16.9	−0.2	13.5
MIROC6	6.6	11.5	−0.2	2.4
Ensemble of 10	−17.2	9.7	−0.3	6.3
EC Earth3	−52.0	19.9	−0.1	18.9
MPI-ESM1-2-HR	−51.7	19.6	0.0	18.8

Table 3
Kurtosis Skewness of extreme precipitation series.

CMIP6	Kurtosis (k)	Remark	Skewness (g)	Remark
CHIRPS	−0.62	Platykurtic	−0.07	Negative skewness
BCC-CSM2-MR	2.40	Leptokurtic	1.32	Positive skewness
CESM2-WACCM	−0.23	Platykurtic	0.69	Positive skewness
GFDL-ESM4	3.55	Leptokurtic	1.61	Positive skewness
GFDL-CM4	−0.13	Platykurtic	0.43	Positive skewness
INM-CM5-0	−0.70	Platykurtic	0.54	Positive skewness
MRI-ESM2-0	0.09	Leptokurtic	0.34	Positive skewness
NorESM2-MM	1.14	Leptokurtic	0.64	Positive skewness
ACCESS-ESM1-5	−0.74	Platykurtic	0.25	Positive skewness
CMCC-ESM2	3.67	Leptokurtic	1.87	Positive skewness
MIROC6	2.48	Leptokurtic	0.99	Positive skewness
Ensemble	−0.46	Platykurtic	0.69	Positive skewness

ESM4, and CMCC-ESM2 were highly skewed (Table 3). This means that these models estimated high values of extreme precipitation than others.

3.3. Probable distribution function (PDF) selections

The goodness-of-fit test shows that the best fit distribution varies from model to model. No single distribution consistently fits well. The likelihood estimation method was used to estimate the distribution method's parameters. The distribution with the lowest sum of the three methods' ranks was considered the best-fit distribution. The KS test and AD show the same rank for most models when choosing a possible frequency method. General generalized extreme values (GEV) have the highest ranking using the K–S and A-D tests. However, using the C–S test, the GUM has ranked first. For the most part, GEV outperformed all other approaches, followed by the GUM distribution method (Table 4). GEV distribution was also reported as a robust model for frequency analysis in the Nile River basin of Ethiopia [58]. According to Tegegne et al. [58], GEV is the best for flood frequency analysis over the Blue Nile basin based on K–S and A-D test statistics. This might be because, despite their distinct hydrological conditions, Abbay and Awash River basins have a number of similar environmental, spatial, and temporal characteristics. Both basins experience a unimodal precipitation distribution with the majority of rainfall occurring during the summer season but with pronounced seasonal variations. Additionally, they are subject to the influence of the Ethiopian Highlands, which play a pivotal role in determining the overall hydrology of the regions. The rugged terrain and highlands surrounding these basins contribute to the formation of numerous tributaries and an intricate network of rivers, influencing the flow patterns and water availability.

Similarly, other studies conducted on analyzing extreme precipitation in different parts of the world described as GEV is the best fit techniques [12,16,26,59]. Therefore, this study used GEV values to investigate intense precipitation's return period and cumulative frequency function.

Fig. 2 depicts a plot of a fitted PDF using CMIP6 models. ACCESS-ESM1-5, GFDL-CM4, and MRI-ESM2-0, probable frequency methods show a normal empirical distribution around the mean (Fig. 2a, f, and j). Some models had a larger frequency of incidents (Fig. 2b, c, e, and g). In extreme precipitation CMCC-ESM2 and BCC-CSM2-MR, GEV shows a higher frequency of incidents (Fig. 2e). All frequency approaches evaluated with CMCC-ESM2 show a low frequency of extreme precipitation above 40 mm (Fig. 2e). The frequency assessments for various climate models reveal distinct precipitation patterns. CHIRPS and MIROC6 consistently project a high likelihood of rainfall events ranging from 36 to 40 mm (Fig. 2d and i). In contrast, the INM-CM5-0 model anticipates a notable probability of rainfall within the 24–26 mm range (Fig. 2h). NorESM2-MM indicates no likelihood of rainfall exceeding 40 mm (Fig. 2k). The Ensemble model foresees the highest probability of maximum rainfall at 37 mm (Fig. 2l).

Table 4
Selection method of probability frequency methods.

Model name	K–S test	A-D test	C–S test	Rank (sum)
ACCESS-ESM1-5	GEV (0.074)	GEV (0.181)	GEV (0.0678)	GEV (3)
BCC-CSM2-MR	GUM (0.102)	GEV (0.304)	GEV (1.214)	GEV (4)
CESM2-WACCM	GEV (0.115)	GEV (0.300)	GUM (1.766)	GEV (5)
CHIRPS	GEV (0.107)	GEV (0.281)	LN (0.170)	GEV (5)
CMCC-ESM2	GEV (0.107)	GEV (0.371)	GUM (2.14)	GEV (6)
GFDL-ESM4	GEV (0.105)	GEV (0.253)	GEV (0.432)	GEV (3)
GFDL-CM4	GUM (0.099)	GEV (0.340)	GUM (0.045)	GUM (6)
INM-CM5-0	Weib (0.107)	GEV (0.453)	N (0.468)	GEV (6)
MIROC6	Weib (0.068)	LN (0.253)	N (0.054)	LN (7)
MRI-ESM2-0	LN (0.097)	GAM (0.331)	N (1.230)	LN (7)
NorESM2-MM	Weib (0.119)	GAM (0.448)	LN (0.65)	GAM (7)
Ensemble	GEV (0.087)	GEV (0.276)	GUM (0.543)	GEV (4)
Highest Rank in %	GEV (50 %)	GEV (75 %)	GUM (33 %)	GEV (75 %)

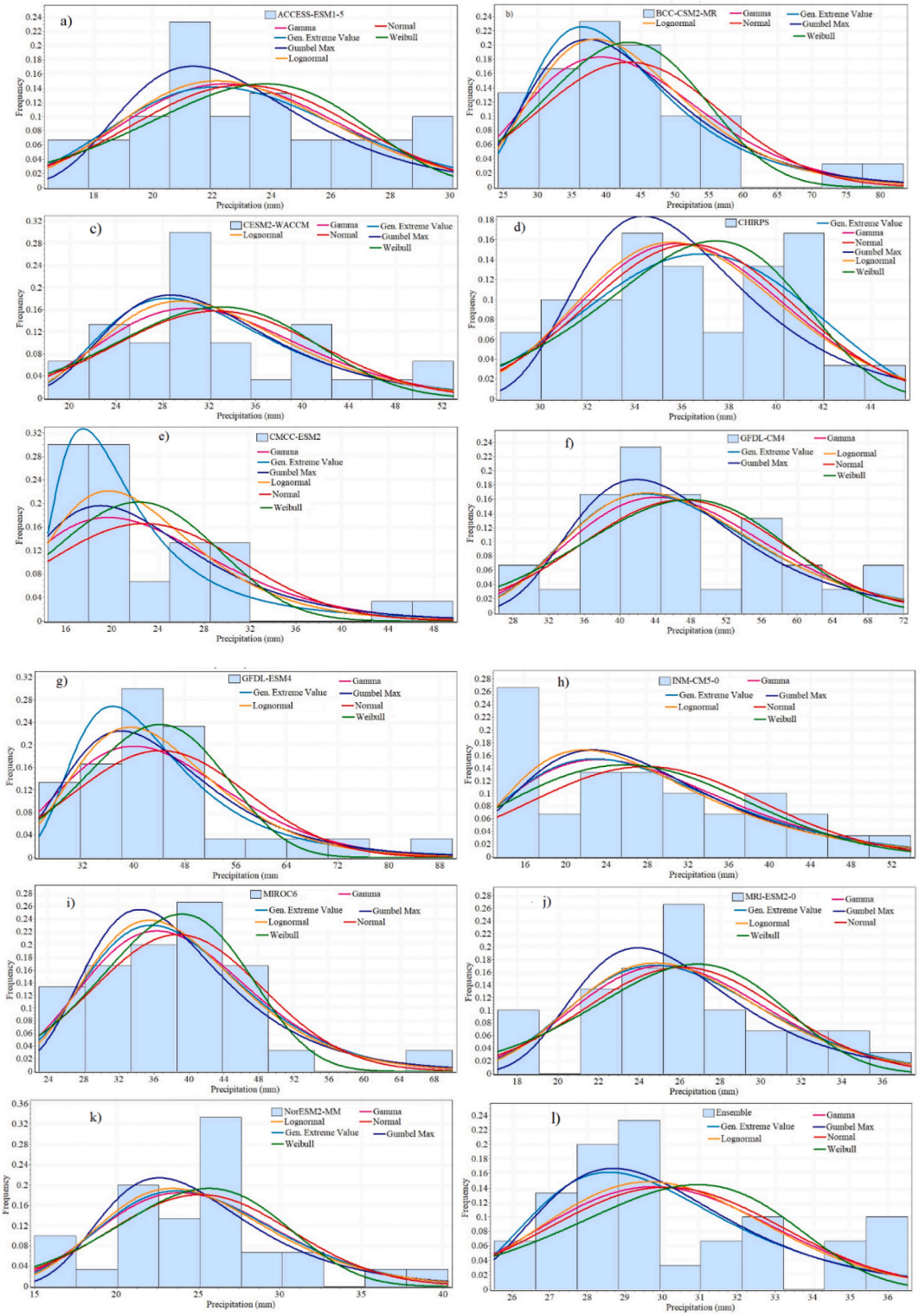

Fig. 2. Histogram of extreme rainfall and fitted PDF of ACCESS-ESM1-5 (a), BCC-CSM2-MR (b), CESM2-WACCM (c), CHIRPS (d), CMCC-ESM2 (e), GFDL-CM4 (f), GFDL-ESM4 (g), INM-CM5-0 (h), MIROC6 (i), MRI-ESM2-0 (j), NorESM2-MM (k) and Ensemble (l).

3.4. Quantile-quantile plots (Q-Q plots)

The low probability extreme events in the right tail were characterized using the Q-Q plot of probability distribution fitting. The Q-Q graphs were created for all models using the generalized extreme value. For the models indicated in Fig. 3a, c, e, f, and l low precipitation values fall on the line while for the models BCC-CSM2-MR, GFDL-ESM4, INM-CM5-0, CHIRPS, MIROC6 and MRI-ESM2-0, this is not the case (Fig. 3b, g, h, d, i, j)In the ACCESS-ESM1-5 (Fig. 3a) model, precipitation values between 16 mm and 28 mm are on the [1:1] line. In MIROC6 and NorESM2-MM, GEV underestimated the right tail and overestimated the high values (Fig. 3i and k). The GEV accurately predicted the average precipitation and could not predict the precipitation on the left and right tail of the INM-CM5-0 (Fig. 3h). Fig. 3 shows a Q-Q plot using GEV.

3.5. Extreme precipitation event

GEV worked well with most models in the goodness of fit test. It estimates the probability of extreme precipitation for the maximum daily precipitation for the 5-year, 10-year, 15-year, 25-year, 50-year, and 100-year return periods. The return periods were underestimated by the MRI-ESM2-0, NorESM2-MM, ACCESS-ESM1-5, and CMCC-ESM2. The CMCC-ESM2 estimated a 100-year return period better than the 5-year return period for extreme precipitation. GFDL-ESM4, BCC-CSM2-MR, and GFDL-CM4 estimated high values of extreme rainfall. The lowest values of severe precipitation were predicted with access-ESM1-5 and then the ensemble (Fig. 4).

The probability of extreme precipitation greater than 50 mm/day is unlikely over the Awash River basin in the Ensemble, CHIRPS, MRI-ESM2-0, NorESM2-MM, ACCESS-ESM1-5, and CMCC-ESM2 models. The probability of the highest extreme precipitation is high in the GFDL-ESM4, BCC-CSM2-MR, and BCC-CSM2-MR models (Fig. 5).

In ACCESS-ESM1-5 and CMCC-ESM2 models, extreme rainfall greater than 25 mm is unlikely. CHIRPS has extreme rainfall between 50 mm/day and 25 mm/day, while GFDL-ESM4 has extreme rainfall between 35 mm/day to 90 mm/day. From the GCMs, the probability of extreme precipitation to occur in MIROC6 and CESM2-WACCM was simulated better than in CHIRPS. The commutative distribution of extreme precipitation is shown in Fig. 5.

3.6. Spatial distribution of extreme rainfall

Based on the Statistical models' performance, ten models and their ensembles were chosen to analyze the spatial distribution of

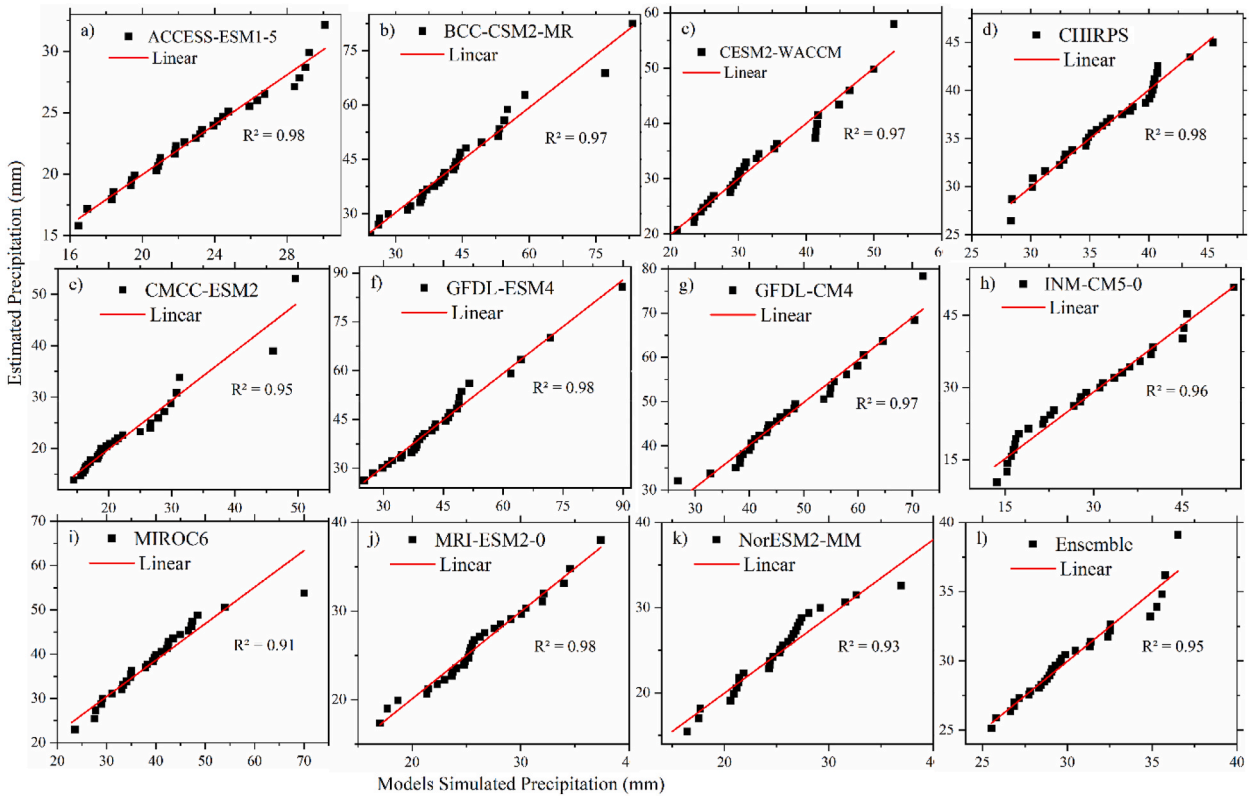

Fig. 3. Q-Q plot using GEV for ACCESS-ESM1-5 (a), BCC-CSM2-MR (b), CESM2-WACCM (c), CHIRPS (d), CMCC-ESM2 (e), GFDL-ESM4 (g), GFDL-CM4 (f), INM-CM5-0 (h), MIROC6 (i), MRI-ESM2-0 (j), NorESM2-MM (k) and Ensemble (l).

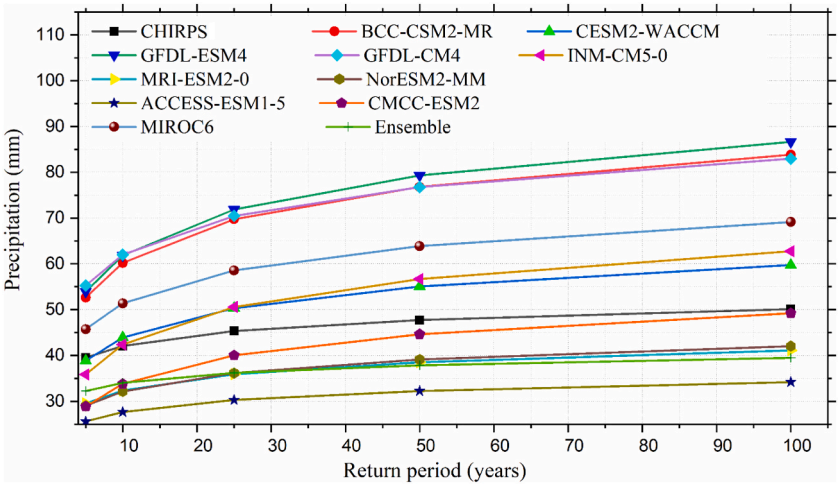

Fig. 4. Annual extreme rainfall and return period over the Awash Basin.

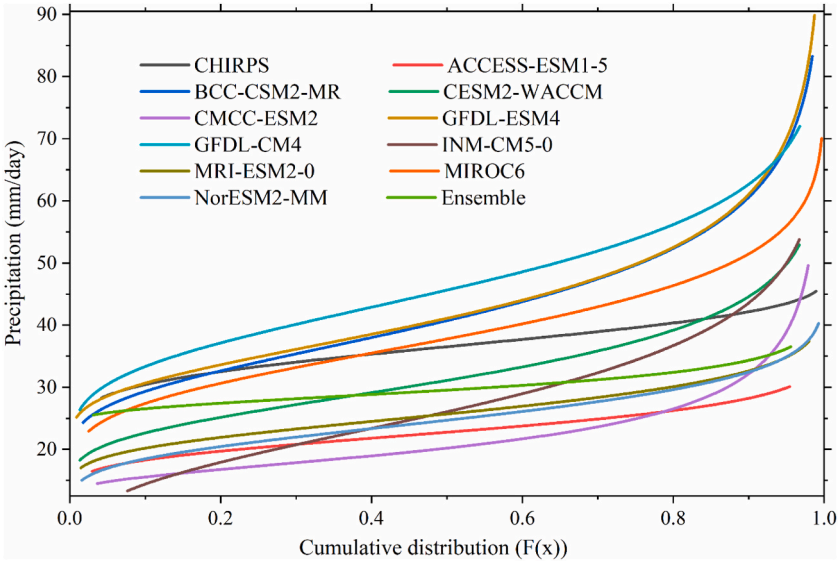

Fig. 5. Cumulative distribution.

extreme rainfall over the Awash basin. Fig. 6 depicts the selected models, and the CHIRPS simulated data spatial distribution. The GFDL-ESM4, Ensemble, and ACCESS-ESM1-5 models simulated data across a large area with uniform peak rainfall (Fig. 6 g, 6l and 6 b, respectively). CMCC-ESM2, MRI-ESM2-0, NorESM2-MM, and ACCESS-ESM1-5 models projected the lowest recorded rainfall (Fig. 6e, j, k, b), whereas BCC-CSM2-MR (Fig. 6c) model forecasted an exceptionally high value in contrast to the CHIRPS (Fig. 6a). CESM2-WACCM predicts the highest maximum rainfall at 95 mm (Fig. 6d), while GFDL-CM4 anticipates slightly less at 80 mm (Fig. 6f). INM-CM5-0 foresees a maximum rainfall of 70 mm (Fig. 6h), and MIROC6 falls on the higher end of the spectrum with an estimated maximum of around 105 mm (Fig. 6i).

Peak rainfall simulated by BCC-CSM2-MR, CHIRPS, and MIROC6 varied substantially. CMCC-ESM2, MRI-ESM2-0, NorESM2-MM, and ACCESS-ESM1-5 simulated the lowest rainfall value, whereas BCC-CSM2-MR simulated a very high value when compared to the CHIRPS model that simulated extreme rainfall data. Most of the models simulated well in the upstream and biased in the downstream of the watershed. The finding is in line with the study report by Ref. [40] who reported that models have shown better correlation on the upstream than the downstream areas. This is mainly due the fact that precipitation simulation is sensitive to orography with under estimation in lower areas. The special extreme precipitation simulated by models CESM2-WACCM, INM-CM5-0, and ACCESS-ESM1-5 is similar to that of extreme precipitation simulated by CHIRPS.

Overall, the study has a few limitations. Firstly, the study looked only at the historical data from the climate models (1985–2014). In the future, researchers could study a longer time future projection to get a better understanding of how extreme weather patterns change over time. Secondly, the study mainly used one source of observed data, which might have some inaccuracies. The use of

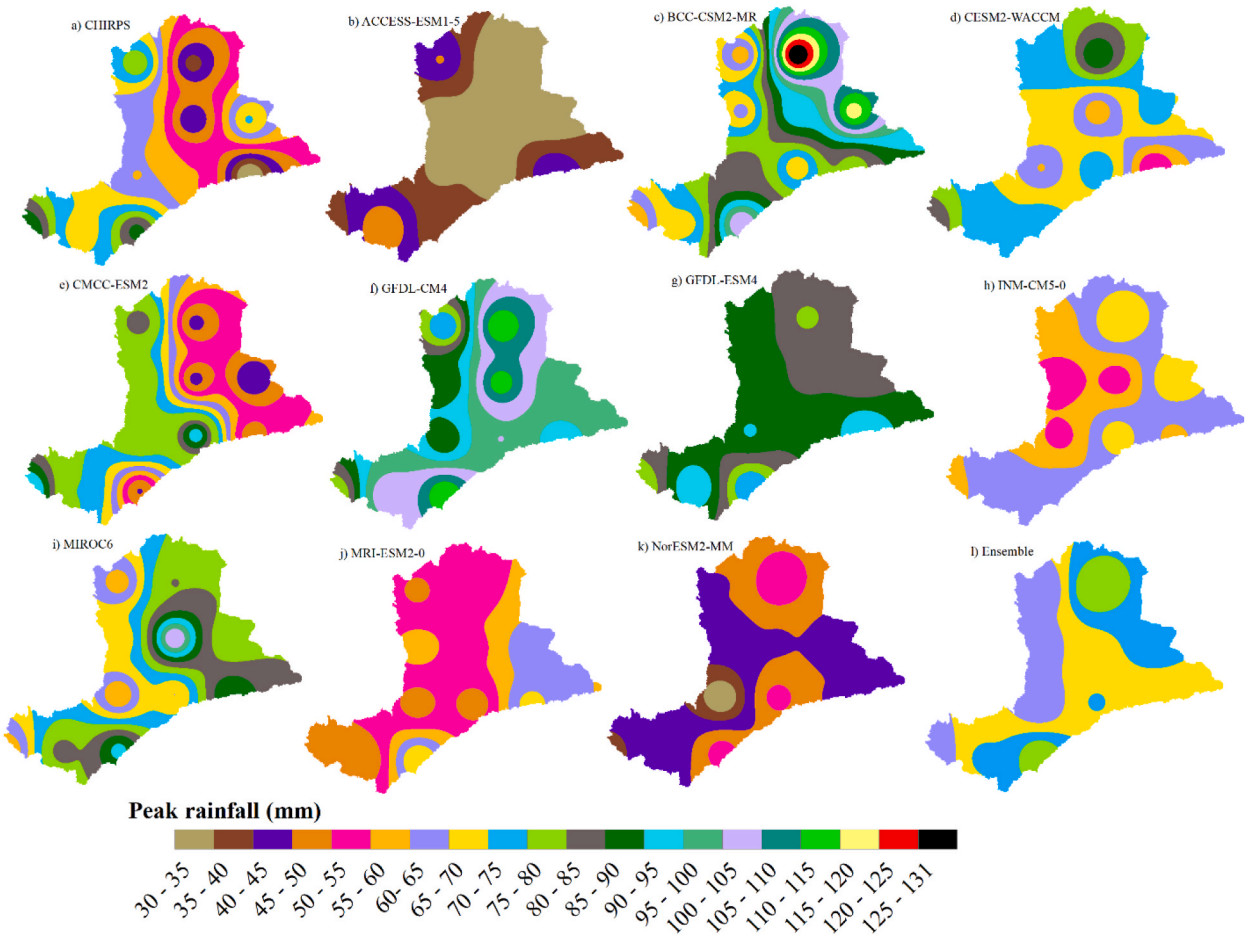

Fig. 6. Spatial distribution of extreme rainfall over Awash Basin under CHIRPS (a), ACCESS-ESM1-5 (b), BCC-CSM2-MR (c), CESM2-WACCM (d), CMCC-ESM2 (e), GFDL-CM4 (f), GFDL-ESM4 (g), INM-CM5-0 (h), MIROC6 (i), MRI-ESM2-0 (j), NorESM2-MM (k) and Ensemble (l).

multiple sources and advanced methods can make a better estimate of extreme weather. Finally, the study's findings are specific to one river basin in Ethiopia. Doing similar studies in different places with different agro ecology can help us know if the methods used work well everywhere.

4. Conclusion

Extreme precipitation is used to design hydraulic structures such as Dam, dam spillways, flood control structures, bridges, and weirs. Therefore, it is required to know the information on the data source used to analyze the extreme rainfall. So here, we evaluated the CMIP6 models in simulating extreme precipitation data. It was found that all models did not equally perform in the extreme precipitation analysis. The MIDROC6 model is better performed than all others in extreme precipitation simulation. It would be used to analyze extreme precipitation.

The best fit probable distribution function is used to select the model that will be used to forecast the extreme precipitation or probable maximum precipitation at a given period. The study found that the GEV is the best fit probable distribution function of all others. It is used in extreme precipitation events for 5-year, 10-year, 15-year, 25-year, 50-year, and 100 years. In general, the GFDL-ESM4 model simulated very high extreme precipitation, ACCESS-ESM1-5 simulated very low extreme precipitation, and MIDROC performed well and was recommended for the extreme precipitation forecast design.

Funding

This study received no outside funding.

Data availability statement

Data will be made available on request from the corresponding author.

Additional information

No additional information is available for this paper.

CRediT authorship contribution statement

Chala Hailu Sime: Writing – review & editing, Writing – original draft, Methodology, Data curation, Conceptualization. **Wakjira Takala Dibaba:** Writing – review & editing, Supervision, Formal analysis, Conceptualization.

Declaration of competing interest

The authors declare that they have no known competing financial interests or personal relationships that could have appeared to influence the work reported in this paper.

Acknowledgements

We would like to thank Jimma Institute of Technology, Center of Excellence in Science and Technology,Jimma University, Ethiopia for the partial support they provided for this research. We extend our thanks to the Earth System Grid Federation for generously providing the CMIP6 data. Additionally, we would like to recognize the CMIP6 data source website: https://esgf-node.llnl.gov/projects/cmip6/. Our sincere gratitude goes to Prof. Dr. A. Venkata Ramayya, JiT ExiST CoE, for his invaluable guidance.

References

[1] E. Elahi, Z. Khalid, Z. Zhang, Understanding farmers' intention and willingness to install renewable energy technology: a solution to reduce the environmental emissions of agriculture, Appl. Energy 309 (2022), 118459.
[2] A. Abbas, M. Waseem, R. Ahmad, K.A. Khan, C. Zhao, J. Zhu, Sensitivity analysis of greenhouse gas emissions at farm level: case study of grain and cash crops, Environ. Sci. Pollut. Control Ser. 29 (54) (2022) 82559–82573.
[3] A. Abbas, C. Zhao, M. Waseem, R. Ahmad, Analysis of energy input–output of farms and assessment of greenhouse gas emissions: a case study of cotton growers, Front. Environ. Sci. 9 (2022), 826838.
[4] E. Elahi, Z. Khalid, M.Z. Tauni, H. Zhang, X. Lirong, Extreme weather events risk to crop-production and the adaptation of innovative management strategies to mitigate the risk: a retrospective survey of rural Punjab, Pakistan, Technovation 117 (2022), 102255.
[5] A. Srivastava, R. Grotjahn, P.A. Ullrich, Evaluation of historical CMIP6 model simulations of extreme precipitation over contiguous US regions, Weather Clim. Extrem. 29 (2020), 100268, https://doi.org/10.1016/j.wace.2020.100268.
[6] Y. Wu, C. Miao, Y. Sun, A. AghaKouchak, C. Shen, X. Fan, Global observations and CMIP6 simulations of compound extremes of monthly temperature and precipitation, GeoHealth 5 (2021) 1–13, https://doi.org/10.1029/2021GH000390.
[7] H.Y. Zheng, C.Y. Miao, J.W. Wu, X.H. Lei, W.H. Liao, H. Li, Temporal and spatial variations in water discharge and sediment load on the Loess Plateau, China: a high-density study, Sci. Total Environ. 666 (2019) 875–886.
[8] J.J. Gou, C.Y. Miao, Q.Y. Duan, Q.H. Tang, Z.H. Di, W.H. Liao, J.W. Wu, R. Zhou, Sensitivity analysis-based automatic parameter calibration of the variable infiltration capacity (VIC) model for streamflow simulations over China Water Resour, Res. 56 (2020), e2019WR025968.
[9] A.O. Lima, G.B. Lyra, M.C. Abreu, J.F. Oliveira-Júnior, M. Zeri, G. Cunha-Zeri, Extreme rainfall events over Rio de Janeiro State, Brazil: characterization using probability distribution functions and clustering analysis, Atmos. Res. 247 (2021), 105221, https://doi.org/10.1016/j.atmosres.2020.105221.
[10] A. Kassegn, E. Endris, Review on socio-economic impacts of 'triple threats' of COVID-19, desert locusts, and floods in East Africa: evidence from Ethiopia, Cogent Social Sciences 7 (1) (2021), 1885122.
[11] S.Y. Tola, A. Shetty, Extreme hydroclimatic variability and impact of local and global climate system anomalies on extreme flow in the Upper Awash River basin, Theor. Appl. Climatol. (2023) 1–21.
[12] M. Alam, K. Emura, C. Farnham, J. Yuan, Best-fit probability distributions and return periods for maximum monthly rainfall in Bangladesh, Climate 6 (1) (2018) 9, https://doi.org/10.3390/cli6010009.
[13] R.A. Warren, C. Jakob, S.M. Hitchcock, B.A. White, Heavy versus extreme rainfall events in southeast Australia, Q. J. R. Meteorol. Soc. 147 (739) (2021) 3201–3226.
[14] S. Das, D. Zhu, C.-H. Cheng, A regional approach of decadal assessment of extreme precipitation estimates: a case study in the yangtze River Basin, China, Pure Appl. Geophys. 177 (2) (2019) 1079–1093, https://doi.org/10.1007/s00024-019-02354-6.
[15] S. Das, D. Zhu, Y. Yin, Comparison of mapping approaches for estimating extreme precipitation of any return period at ungauged locations, Stoch. Environ. Res. Risk Assess. 34 (8) (2020) 1175–1196, https://doi.org/10.1007/s00477-020-01828-7.
[16] J. Yuan, K. Emura, C. Farnham, M.A. Alam, Frequency analysis of annual maximum hourly precipitation and determination of best fit probability distribution for regions in Japan, Urban Clim. 24 (2018) 276–286, https://doi.org/10.1016/j.uclim.2017.07.008.
[17] A.A. Akinsanola, V. Ongoma, G.J. Kooperman, Evaluation of CMIP6 models in simulating the statistics of extreme precipitation over Eastern Africa, Atmos. Res. 254 (2021) 1–12, https://doi.org/10.1016/j.atmosres.2021.105509.
[18] Z. Li, C. Li, Z. Xu, X. Zhou, Frequency analysis of precipitation extremes in Heihe River basin based on generalized Pareto distribution, Stoch. Environ. Res. Risk Assess. 28 (7) (2013) 1709–1721, https://doi.org/10.1007/s00477-013-0828-5.
[19] V. Eyring, S. Bony, G.A. Meehl, C.A. Senior, B. Stevens, R.J. Stouffer, K.E. Taylor, Overview of the coupled model intercomparison project phase 6 (CMIP6) experimental design and organization, Geosci. Model Dev. (GMD) 9 (5) (2016) 1937–1958.
[20] C.-A. Chen, H.-H. Hsu, H.-C. Liang, Evaluation and comparison of CMIP6 and CMIP5 model performance in simulating the seasonal extreme precipitation in the western north pacific and East asia, Weather Clim. Extrem. (2020), https://doi.org/10.1016/j.wace.2021.100303.
[21] A. Abbas, M. Waseem, R. Ahmad, K.A. Khan, C. Zhao, J. Zhu, Sensitivity analysis of greenhouse gas emissions at farm level: case study of grain and cash crops, Environ. Sci. Pollut. Control Ser. 29 (54) (2022) 82559–82573.
[22] A. Abbas, A.S. Bhatti, S. Ullah, W. Ullah, M. Waseem, C. Zhao, X. Dou, G. Ali, Projection of precipitation extremes over south asia from CMIP6 GCMs, Journal of Arid Land 15 (3) (2023) 274–296.

[23] S.H. Gebrechorkos, C. Bernhofer, S. Hülsmann, Climate change impact assessment on the hydrology of a large river basin in Ethiopia using a local-scale climate modelling approach, Sci. Total Environ. 742 (2020) 1–13, https://doi.org/10.1016/j.scitotenv.2020.140504.

[24] M.T. Taye, E. Dyer, F.A. Hirpa, K. Charles, Climate change impact on water resources in the Awash Basin, Ethiopia, Water 10 (2018) 1–16, https://doi.org/10.3390/w10111560.

[25] J. Liu, C.D. Doan, S.-Y. Liong, R. Sanders, A.T. Dao, T. Fewtrell, Regional frequency analysis of extreme rainfall events in Jakarta, Nat. Hazards 75 (2) (2014) 1075–1104, https://doi.org/10.1007/s11069-014-1363-5.

[26] A.A. Al Mamoon, A. Rahman, Selection of the best fit probability distribution in rainfall frequency analysis for Qatar, Nat. Hazards 86 (1) (2016) 281–296, https://doi.org/10.1007/s11069-016-2687-0.

[27] S.R. Chavan, V.V. Srinivas, Evaluation of three approaches to probable maximum precipitation estimation: a study on two Indian river basins, Theor. Appl. Climatol. 144 (1–2) (2021) 731–749, https://doi.org/10.1007/s00704-021-03557-5.

[28] C. Mo, Y. Ruan, J. He, J. Jin, P. Liu, G. Sun, Frequency analysis of precipitation extremes under climate change, Int. J. Climatol. 39 (3) (2018) 1373–1387, https://doi.org/10.1002/joc.5887.

[29] D. Tong, J. Cheng, Y. Liu, S. Yu, L. Yan, C. Hong, Y. Qin, H. Zhao, Y. Zheng, G. Geng, M. Li, Dynamic projection of anthropogenic emissions in China: methodology and 2015–2050 emission pathways under a range of socio-economic, climate policy, and pollution control scenarios, Atmos. Chem. Phys. 20 (9) (2020) 5729–5757.

[30] T. Fiedler, A.J. Pitman, K. Mackenzie, N. Wood, C. Jakob, S.E. Perkins-Kirkpatrick, Business risk and the emergence of climate analytics, Nat. Clim. Change 11 (2) (2021) 87–94.

[31] B. Ayugi, V. Dike, H. Ngoma, H. Babaousmail, R. Mumo, V. Ongoma, Future changes in precipitation extremes over East Africa based on CMIP6 models, Water 13 (17) (2021) 2358.

[32] M. Fazzini, C. Bisci, P. Billi, The Climate of Ethiopia, World Geomorphological Landscapes, 2015, pp. 65–87.

[33] M. Almazroui, F. Saeed, S. Saeed, M.N. Islam, M. Ismail, N.A.B. Klutse, M.H. Siddiqui, Projected change in temperature and precipitation over Africa from CMIP6, Earth Systems and Environment 4 (3) (2020) 455–475, https://doi.org/10.1007/s41748-020-00161-x.

[34] T. Dinku, C. Funk, P. Peterson, R. Maidment, T. Tadesse, H. Gadain, P. Ceccato, Validation of the CHIRPS satellite rainfall estimates over eastern, Q. J. R. Meteorol. Soc. 144 (2018) 292–312, https://doi.org/10.1002/qj.3244.

[35] N. Scafetta, CMIP6 GCM validation based on ECS and TCR ranking for 21st century temperature projections and risk assessment, Atmosphere 14 (2) (2023) 345.

[36] D. Berhanu, T. Alamirew, M.T. Taye, D. Tibebe, S. Gebrehiwot, G. Zeleke, Evaluation of CMIP6 models in reproducing observed rainfall over Ethiopia, Journal of Water and Climate Change 14 (8) (2023) 2583–2605.

[37] A. Salazar, M. Thatcher, K. Goubanova, P. Bernal, J. Gutiérrez, F. Squeo, CMIP6 precipitation and temperature projections for, Chile (2023), https://doi.org/10.21203/rs.3.rs-3007072/v1.

[38] J. Zhou, J. Zhao, An intercomparison between ERA-interim reanalysis and observed precipitation in northeast China, Discrete Dynam Nat. Soc. (2015) 1–9, https://doi.org/10.1155/2015/693923, 2015.

[39] Ramesh S.V. Teegavarapu, Tadesse Meskele, Chandra S. Pathak, Geo-spatial grid-based transformations of precipitation estimates using spatial interpolation methods 40 (none) (2012) 28–39, https://doi.org/10.1016/j.cageo.2011.07.004.

[40] W.T. Dibaba, K. Miegel, T.A. Demissie, Evaluation of the CORDEX regional climate models performance in simulating climate conditions of two catchments in Upper Blue Nile Basin, Dynam. Atmos. Oceans 87 (2019), 101104, https://doi.org/10.1016/j.dynatmoce.2019.101104.

[41] V. Ongoma, H. Chen, C. Gao, Evaluation of CMIP5 twentieth century rainfall simulation over the equatorial East Africa, Theor. Appl. Climatol. (2018), https://doi.org/10.1007/s00704-018-2392-x.

[42] T. Chai, R.R. Draxler, Root mean square error (RMSE) or mean absolute error (MAE)? – Arguments against avoiding RMSE in the literature, Geosci. Model Dev. (GMD) 7 (3) (2014) 1247–1250.

[43] T.A. Demissie, C.H. Sime, Assessment of the performance of CORDEX regional climate models in simulating rainfall and air temperature over southwest Ethiopia, Heliyon 7 (8) (2021), e07791, https://doi.org/10.1016/j.heliyon.2021.e07791.

[44] C.H. Sime, T.A. Demissie, Assessment and prediction of the climate change impact on crop yield, in Jimma zone upper gilgel gibe districts, Ethiopia, Arabian J. Geosci. 15 (3) (2022) 313.

[45] S. Yue, T.B.M. Ouarda, B. Bobée, P. Legendre, P. Bruneau, The Gumbel mixed model for flood frequency analysis, J. Hydrol. 226 (1–2) (1999) 88–100, https://doi.org/10.1016/s0022-1694(99)00168-7.

[46] N.N. Daba, T.A. Demissie, C.H. Sime, Probable maximum precipitation estimation using Hershfield's statistical method: a case of Dedessa sub-basin, Ethiopia, Modeling Earth Systems and Environment (2021), https://doi.org/10.1007/s40808-021-01228-y.

[47] R.D. Markovic, Probability Functions of Best Ft to Distributions of Annual Precipitation and Runof, Doctoral dissertation, Colorado State University, Libraries), 1965.

[48] Z. Şen, A.G. Eljadid, Rainfall distribution function for Libya and rainfall prediction, Hydrol. Sci. J. 44 (5) (1999) 665–680, https://doi.org/10.1080/02626669909492266.

[49] G.B. Lyra, B.I.L. Garcia, S.M.D.S. Piedade, G.C. Sediyama, P.C. Sentelhas, Regiões homogêneas e funções de distribuição de probabilidade da precipitação pluvial no Estado de Táchira, Venezuela, Pesqui. Agropecuária Bras. 41 (2) (2006) 205–215, https://doi.org/10.1590/S0100-204X2006000200004.

[50] J.R. Stendinger, R.M. Vogel, E. Foufoula-Georgiou, Frequency analysis of extreme events, in: D.A. Maidment (Ed.), Handbook of Hydrology, first ed., McGraw-Hill, New York, NY, USA, 1993, 0070397325.

[51] J.L. Salinas, A. Castellarin, S. Kohnová, T.R. Kjeldsen, Regional parent flood frequency distributions in Europe – Part 2: climate and scale controls, Hydrol. Earth Syst. Sci. 18 (11) (2014) 4391–4401, https://doi.org/10.5194/hess-18-4391-2014.

[52] M.C. Abreu, R.A. Cecílio, F.F. Pruski, G.R. dos Santos, L.T. de Almeida, S.S. Zanetti, Critérios para Escolha de Distribuições de Probabilidades em Estudos de Eventos Extremos de Precipitação, Revista Brasileira de Meteorologia 33 (4) (2018) 601–613, https://doi.org/10.1590/0102-7786334004.

[53] J.C.F. Melo Júnior, G.C. Sediyama, P.A. Ferreira, B.G. Leal, Determinação de regiões homogêneas quanto à distribuição de freqüência de chuvas no leste do Estado de Minas Gerais, Rev. Bras. Eng. Agrícola Ambient. 10 (2006) 408–416, https://doi.org/10.1590/S1415-43662006000200023.

[54] W.J. Conover, Practical Nonparametric Statistics, third ed., John Wiley & Sons, Inc., New York, NY, USA, 1999, pp. 428–433, 0471160687.

[55] C.A. Sansigolo, Distribuições de extremos de precipitação diária, temperatura máxima e mínima e velocidade do vento em Piracicaba, SP (1917-2006), Rev. Bras. Meteorol. 23 (2008) 341–346, https://doi.org/10.1590/S0102-77862008000300009.

[56] A. J. de Oliveira Júnior, S. R. L. de Souza, E. Dal Pai, B.T. Rodrigues, V. C. de Souza, Aurora: mobile application for analysis of spatial variability of thermal comfort indexes of animals and people, using IDW interpolation, Comput. Electron. Agric. 157 (2019) 98–101, https://doi.org/10.1016/j.compag.2018.12.029.

[57] C.L. Chang, S.L. Lo, S.L. Yu, Applying fuzzy theory and genetic algorithm to interpolate precipitation, J. Hydrol. 314 (1–4) (2005) 92–104, https://doi.org/10.1016/j.jhydrol.2005.03.034.

[58] G. Tegegne, A.M. Melesse, D.H. Asfaw, A.W. Worqlul, Flood frequency analyses over different basin scales in the Blue nile River Basin, Ethiopia, Hydrology 7 (44) (2020) 1–21, https://doi.org/10.3390/hydrology7030044.

[59] S. Planton, M. Déqué, F. Chauvin, L. Terray, Expected impacts of climate change on extreme climate events, Compt. Rendus Geosci. 340 (9–10) (2008) 564–574, https://doi.org/10.1016/j.crte.2008.07.009.